Biochimica et Biophysica Acta, 1060 (1991) 210–223

ADONIS 0005272891002333

BBABIO 43485

An extended dynamic model of oxidative phosphorylation

Bernard Korzeniewski and Wojciech Froncisz

Institute of Molecular Biology; Jagiellonian University, Kraków (Poland)

(Received 22 January 1991)
(Revised manuscript received 23 May 1991)

Key words: Dynamic model; Oxidative phosphorylation; Thermodynamics; Respiration

The presented model based on an earlier one (Korzeniewski, B. and Froncisz, W. (1989) Studia Biophys. 132, 173–187) simulates concentration changes in time of chemical compounds and thermodynamic forces during respiration of cell suspension in a closed chamber. A set of differential equations solved numerically describes the utilization of oxygen up to anaerobiosis and the behaviour of the system after a sudden pulse of oxygen. Flux control coefficients for most important reactions (enzymes) of oxidative phosphorylation were calculated. A good qualitative and (when a direct comparison is possible) quantitative agreement with experimental results can be observed. The following conclusions can be drawn from the simulation: (1) Wilson's steady state model is not in contradiction with sharing of the control over the respiration between some steps and displacement of the ATP/ADP carrier from equilibrium. (2) The overshoot characteristics of the $\Delta\tilde{\mu}_{H^+}$ time-course after reoxygenation can be explained without using the lag-phase kinetics of ATP-synthetase. (3) A 'hot region' (sharp changes of many parameters) can be distinguished when the oxygen concentration approaches zero; only cytochrome oxidase is clearly sensitive on oxygen concentration in all its range. (4) Control over oxidative phosphorylation is shared mainly between inputs of the system (ATP utilization and substrate dehydrogenation) and the proton leak.

Introduction

The oxidative phosphorylation is one of the most important processes in the cell. It utilizes the Gibbs free energy change of the reaction of electron transfer from respiratory substrates to oxygen to synthesize the universal 'energy mediator' ATP. Hydrolysis of this compound enables occurrence of most of the anabolic reactions by coupling with them. A simulation of this process allows to check our current knowledge about the control over it and to gain some new information.

Some models of the oxidative phosphorylation have been developed. Non-equilibrium thermodynamics (NET) and mosaic non-equilibrium thermodynamics (MNET) succesfully describe some properties of the considered system [2,3]. However, we believe that the kinetic paradigm is more elementary and gives, at least potentially, a deeper insight into biochemical systems. Moreover, NET has serious problems with the flux-force linearity. Bohnensack [4,5] has proposed the kinetic model which deals successfully with some properties of oxidative phosphorylation, but only in mitochondrial conditions. The mentioned models are static.

Abbreviations: A1, concentration of the cytochrome oxidase form $a_3^{3+}O_2Cu^{1+} + a_3^{2+}O_2Cu^{2+}$; A2, concentration of the cytochrome oxidase form $a_3^{3+}O_2^{2-}Cu^{2+} + a_3^{3+}Cu^{2+}$; A21, concentration of the cytochrome oxidase form $a_3^{3+}Cu^{2+}$; A3, concentration of the cytochrome oxidase form $a_3^{3+}Cu^{1+}$; A_{2TD}, the pool variable, $2[ATP_{te}] + [ADP_{te}]$; A_{TDM}, the pool variable, $[ATP_{te}] + [ADP_{te}] + [AMP_{te}]$; A_t, total concentration of cytochrome a_3 in suspension; C2, concentration of the reduced form of cytochrome *c*; C3, concentration of the oxidized form of cytochrome *c*; C_t, total concentration of cytochrome *c* in suspension; H_e, external proton concentration; H_i, internal proton concentration; k_x, k_{bx}, forward and backward rate constant of reaction x; K_x, equilibrium constant of reaction x; K_{Dx}, dissociation constant of ligand x; K_{Mx}, Michaelis-Menten constant of reaction x; n_A, number of protons used for synthesis of 1 ATP molecule; N, concentration of the oxidized form of NAD; Nh, concentration of the reduced form of NAD; O2, concentration of molecular oxygen; N_t, total concentration of NAD in suspension; R_{cm}, ratio of cell to mitochondria volume; R_{sc}, ratio of suspension to cell volume; *S*, $2.303RT$; *Z*, $2.303RT/F$.
Subscripts: a, monovalent; b, divalent; e, external; i, internal; f, free; m, magnesium complex; t, total.
In all equations the concentrations of chemical compounds are represented by symbols written without square brackets for clarity and simplicity.

Correspondence: W. Froncisz, Institute of Molecular Biology, Jagiellonian University, Al. Mickiewicza 3, 31-120 Kraków, Poland.

Two dynamic (i.e., describing changes in time) models of oxidative phosphorylation were developed previously. The first, described by Holzhütter et al. [6], based partially on Bohnensack's model, simulated two kinds of experiment with a suspension of isolated mitochondria in state 4: the 'oxygen pulse' and the 'state 3' experiment. In the 'oxygen pulse' experiment mitochondria in the suspension were allowed to respire until they achieved full anaerobiosis. After some time a sudden pulse of oxygen was introduced. Concentration changes of internal protons, ATP, P_i and external protons in time during such an experiment were measured by Ogawa and Lee [7]. A good agreement between the simulation and experiment results was obtained. The overshoot characteristics of $\Delta\tilde{\mu}_{H^+}$ immediately after reoxygenation was explained by a lag-phase kinetics of the ATP synthetase [6]. In the 'state 3' experiment some amount of external ADP was added to the suspension of mitochondria in state 4. The system then passed to state 3 and, after the conversion of almost all ADP into ATP, returned to the state 4. Concentration value courses in time of the same chemical compounds as in previous experiment have been measured by the same authors [7]. The results of the simulation in this case also agreed quite well with the experimental data. This dynamic model involved the proton-motive force and predicted the quantitative values of parameters relatively well. Its main disadvantages were: (1) An oversimplified description of cytochrome *c* oxidase, a lack of time-courses of the reduction of respiratory chain components (cytochrome *c*, cytochrome oxidase forms); (2) Semi-kinetic (thermodynamic) description of many reactions; (3) Unphysiological conditions (isolated mitochondria, state 4); (4) Linear dependence of the proton leak on components of the protonmotive force; (5) A rather outdated kinetic model of the adenine nucleotide translocator.

The second dynamic model of mitochondrial respiration was described in our previous publication [1]. It was based on the static 'steady-state' model developed by Wilson and co-workers [8–10]. This dynamic model simulated the consumption of oxygen in a closed chamber in two systems. System 1 contained a suspension of isolated mitochondria with an artificial donor of electrons (TMPD). In system 2 the respiration of intact cells' suspension was studied. This model successfully predicted qualitative behaviour of time-courses of some parameters (oxygen concentration, degree of cytochrome *c* reduction, phosphorylation potential) when compared with experiments [9,11–13]. There was a good quantitative agreement between apparent K_m values obtained from simulations and experiments [7]. The model described correctly the function of the respiratory chain and gave some information about the behaviour of cytochrome *c* oxidase. The main, very important disadvantage of this model was the fact that all enzymes and reactions between respiratory chain and external phosphorylation potential were treated as a black box (a phenomological relationship between the external [ATP]/[ADP][P_i] ratio and the respiratory chain is used).

In the present paper, an attempt is made to eliminate the disadvantages of earlier models and create a dynamic one which would include the main features of our current knowledge about mechanisms of oxidative phosphorylation control. Some assumptions had to be made when experimental data were insufficient. A thermodynamic fitting is established as one of the main rules of model building (all parameters are adjusted to fulfil the thermodynamic principles). The model takes into account: substrate dehydrogenation, respiratory chain, cytochrome oxidase, protonmotive force, ATP-synthetase, ATP/ADP carrier, phosphate carrier, adenylate kinase, internal and external ATP consumption. In addition, it includes the following processes: binding of magnesium ions by many reagents, dissociation of monovalent phosphate, binding a part of ADP in cytosol, buffering of protons ejected outside the mitochondrium, and the redox equivalents pool.

We assume that the proton leak is uniquely responsible for the changes in the $H^+/2e^-$ stoichiometry, so that there is no proton pump slipping [14,15]. Our model is not able to distinguish between the delocalized and localized proton gradient.

The parameter values used have been obtained under different conditions by different experimental procedures. So we must emphasize that the presented model is only a semi-quantitative one. It does not deal with any particular kind of cells (although most experimental parameters have been taken from hepatocytes). Some simplifications are necessary owing to the simulation of general properties of the cell system and to our limited knowledge.

Time-dependent changes of parameter values are simulated by solving numerically the set of different equations using the Gear procedure [16] designed especially for 'stiff' problems. Programs are written in Microsoft Fortran. The IBM PC/386 compatible computer was used for simulations. Values of chosen parameters are drawn against time.

The results can be compared with experiments already performed and served to project subsequent ones. The presented simulation gives the deeper understanding of the mechanisms which control the process of oxidative phosphorylation.

Model

The presented simulation describes the 'oxygen pulse' experiment in a suspension of respiring cells in a closed chamber. In Fig. 1 the considered system is shown schematically, the spatial dislocation of reac-

tions and metabolites being emphasized. The simulation is started at the moment when the molecular oxygen concentration $[O_2]$ amounts to 240 μM (saturated solution). It was assumed that in the physiological state $3_{(1/2)}$ the electrochemical potential $\Delta\tilde{\mu}_{H^+}$ equal to about 190 mV (45 mV of $-Z\Delta$pH plus 145 mV of $\Delta\Psi$) is built up. In Refs. 17 and 18 the $\Delta\Psi$ value in hepatocytes close to 140–150 mV was measured. The initial respiratory rate v_{RESP} was established as equal to 1 μM O_2/s at a given value of cytochrome c concentration (0.8 μM) in the suspension according to Ref. 12. On the basis of the established values of parameters and those taken from literature all lacking constant and parameter values were calculated.

Volumes of compartments

It is accepted that the value of intramitochondrial space volume equals to 1 μl per 1 mg of protein [6]. We also assume that the cell to mitochondrial volume ratio R_{cm} is equal to 10 [19]. 1 mg of mitochondrial protein contains 0.27 nmol of cytochrome c [20]. Thus, it is possible, at the established cytochrome c concentration in the suspension, to calculate the suspension volume/cell volume ratio R_{sc}, which amounts to about 34. These ratios are needed because the concentration of some compounds is determined in suspension (O_2, cytochrome oxidase, cytochrome c, internal NAD), and others in the cell volume (external protons, ATP, ADP, AMP, P_i) or in the matrix volume (internal protons, ATP, ADP, P_i).

Cytochrome oxidase

The description of the cytochrome oxidase cycle is based on the steady state model [8–10]. The phenomenological dependence of this enzyme kinetics on the $[ATP_{ie}]/[ADP_{ie}][P_{ite}]$ ratio is used, though, in fact, the phosphorylation potential affects the cytochrome oxidase via $\Delta\Psi$ and ΔpH [21]. The standard free energy change of ATP hydrolysis in the cell is different from that in the mitochondria suspension in Wilson's group experiments (a different magnesium ion concentration). Nevertheless, it is partially compensated by the smaller displacement of the ATP/ADP carrier from the equilibrium in these experiments (only one site of coupling, relatively low inorganic phosphate concentration). The

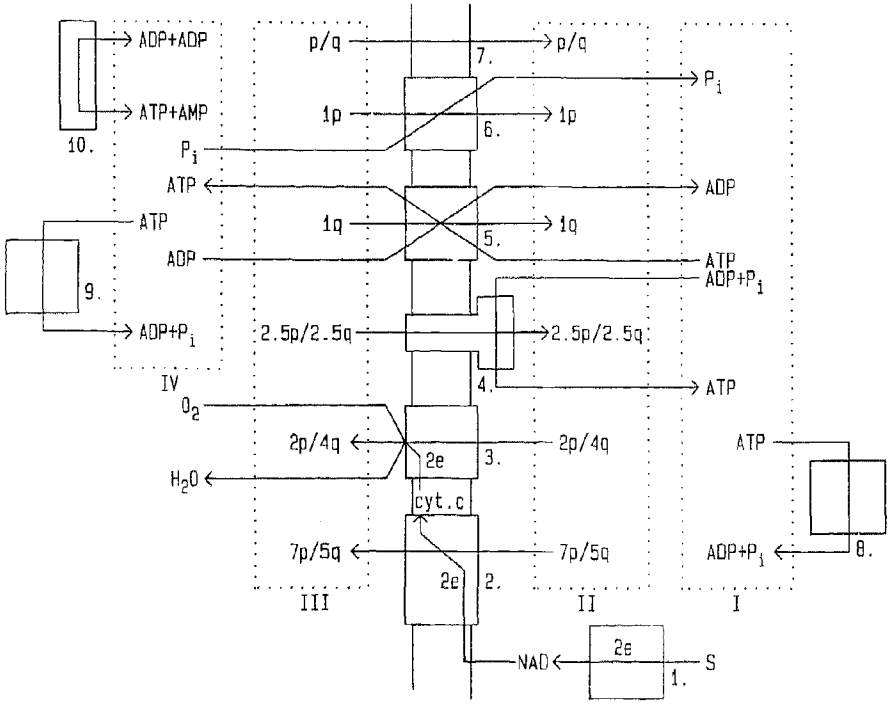

Fig. 1. The system described by the present model. Abbreviations: 1, substrate dehydrogenation; 2, respiratory chain (complex I+III); 3, cytochrome oxidase (complex IV); 4, ATP-synthetase; 5, ATP/ADP carrier; 6, phosphate carrier; 7, proton leak; 8, internal ATP consumption; 9, external ATP utilization; 10, adenylate kinase; I, internal adenine nucleotide and phosphate pool; II, internal proton and charge pool; III, external proton and charge pool; IV, external adenine nucleotide and phosphate pool; p, protons translocated; q, positive charges translocated; e, electrons; S, respiratory substrate.

rates of forward and backward reactions of the cytochrome oxidase cycle are as follows [1]:

$$v_1 = k_1 \cdot A21 \cdot C2 \quad (1)$$

$$v_{b1} = k_{b1} \cdot A3 \cdot C3 \quad (2)$$

$$v_2 = k_2 \cdot A3 \cdot O2 \quad (3)$$

$$v_{b2} = k_{b2} \cdot A1/(1 + K_3) \quad (4)$$

$$v_4 = k_k \cdot A1 \cdot C2 \quad (5)$$

where:

$$A21 = A2/(g + 1) \quad (6)$$

$$g = (C3/C2)^2 \cdot (1/(K_5/AAP)) \quad (7)$$

$$k_k = (k_{4a} + k_{4b} \cdot K_3)/(1 + K_3) \quad (8)$$

$$K_3 = Q \cdot 10^{(E_{ma3} - E_{mCu})/59} \quad (9)$$

$$E_{ma3} = E'_{ma3} - 59 \log_{10}(8 \cdot 10^{-7} + AAP)/(5 \cdot 10^{-3} + AAP) \quad (10)$$

and:

$k_1 = 170\ \mu M^{-1}\ s^{-1}$

$k_{b1} = 5.29 \cdot 10^5 \cdot AAP^{1/2} \mu M^{-1} s^{-1}$

$k_2 = 100\ \mu M^{-1}\ s^{-1}$

$k_{b2} = 1\ s^{-1}$

$k_{4a} = 10\ \mu M^{-1}\ s^{-1}$

$k_{4b} = 150\ \mu M^{-1}\ s^{-1}$

$K_5 = 4$

$Q = 50$

$E'_{ma3} = 170$ mV

$E_{mCu} = 350$ mV

$AAP = [ATP_{ic}]/[ADP_{ic}][P_{i_{ic}}]$

The rate of the cytochrome c oxidation is equal to:

$$v_{OXID} = 2(g(v_1 - v_{b1}) + v_4)/(1 + g) + v_4 + v_1 - v_{b1} \quad (11)$$

The total cytochrome a_3 concentration $A_t = A1 + A2 + A3$ is designed to be equal to 0.4 μM, which corresponds with the established respiratory rate [12]. Thus, the total cytochrome c concentration $C_t = C2 + C3$ amounts to 0.8 μM (about $2A_t$) and the total NAD concentration $N_t = N + Nh$ to 8.8 μM (about $11C_t$) [20]. Initial concentration values of cytochrome c and cytochrome oxidase forms are calculated using the adequate optimization procedure.

Substrate dehydrogenation and respiratory chain

A simple first-order reaction is used for the description of substrate dehydrogenation. It is assumed that its rate depends only on $[NAD^+]$ (constant 'respiratory substrate pool' concentration) and that it is fully irreversible. 'Key enzymes' of the citric acid cycle such as isocitrate dehydrogenase, 2-oxoglutarate dehydrogenase and pyruvate dehydrogenase are reported to be essentially irreversible [22–25]. Their activity is influenced by the concentrations of adenine nucleotides. It has been shown that the rate of reaction catalyzed by 2-oxoglutarate dehydrogenase depends on the [ADP]/[ATP ratio according to the Michaelis-Menten kinetics with the constant K_{MDT} of about 0.2 [25]. Because only a part of the substrate dehydrogenation system depends on the mentioned ratio we assume the value K_{MDT} to be equal to 0.1 for this constant. Since this ratio is always greater than 0.5 under the simulated conditions it can be concluded that adenine nucleotides have rather small influence on substrate dehydrogenation (in accordance with Ref. 18). The rate constant k_d is calculated assuming that the initial substrate dehydrogenation rate $v_{DEHY} = 2v_{RESP}$. Hence:

$$v_{DEHY} = k_d \cdot N(1 + K_{MDT}/(ADP_{ii}/ATP_{ii})) \quad (12)$$

The dependence on the Ca^{2+} concentration is not included because we do not deal with the influence of hormons in the present work.

The respiratory chain between NAD and cytochrome c is assumed to be very close to equilibrium [26]. It is described by the equilibrium constant K_r (a similar effect is given by employing the linear relationship between a flux and a thermodynamic force $J_{redox} = L_{redox} \Delta G_{redox}$ or assuming that the respiratory chain works at a half-maximal rate). On this basis we assume that the electron transfer reaction is displaced from equilibrium to the degree that $v_{forward}/v_{backward}$ equals only 2. The level of cytochrome c reduction is calculated from the thermodynamic span (Gibbs free energy change) between NAD and cytochrome c and from the middle point redox potentials ($E_{mNAD} = -320$ mV, $E_{mcyt.c} = 220$ mV). The thermodynamic span is fixed assuming that the complex I transfers three protons and three charges and the complex III four protons and two charges on each two passing electrons [27]. Thus, at equilibrium, $2\Delta E_{redox} = (7 - 2u) \cdot \Delta\tilde{\mu}_{H^+}$. On this basis, taking into account the assumed displacement from equilibrium, the equilibrium constant K_r is defined as follows:

$$K_r = (C2/C^3)^2 (N/Nh)(H_e/H_i)^{(7-2u)/(1-u)} \quad (13)$$

Generally, it is accepted that the whole respiratory chain transfers nine protons and nine charges across

the inner mitochondrial membrane per two electrons (complex IV: two protons and four charges). Some electrons enter the respiratory chain at the complex II, which leads to a decrease of the overall $H^+/2e^-$ stoichiometry. On the other hand, many authors assess the stoichiometry for the complex I + III as equal to 8, which elicits the opposite result. These effects compensate each other at least partially. For the time-course simulation the level of a cytochrome *c* reduction is calculated at each step from the level of the NAD reduction and the proton-motive force. Buffering of the intramitochondrial NAD pool, mainly by the β-hydroxybutyrate/acetoacetate pair, has been found [28]. On the basis of this work it is assumed that the 'buffered' NAD pool is 5-times larger than the 'real' one.

Protonmotive force and proton leak

It is assumed that, according to the chemiosmotic theory, the protonmotive force $\Delta\tilde{\mu}_{H^+}$ is a 'high energy' mediate between the respiratory chain and the ATP synthesis. This force, being the electrochemical potential, consists of the osmotic ($-Z\Delta$pH) and electrical ($\Delta\Psi$) parts. The linear dependence between components of $\Delta\mu_{H^+}$ is assumed [6,28,29]. Thus, the ratio $u = \Delta\Psi/\Delta\tilde{\mu}_{H^+}$ is kept constant. It is maintained by the relatively fast secondary ions translocation. For aerobic conditions in the state $3_{(1/2)}$ of respiration the following potential values are accepted:

$\Delta\tilde{\mu}_{H^+} = 190$ mV

$\Delta\Psi = 145$ mV

$-Z\Delta\text{pH} = 45$ mV

In the set of differential equations changes in $[H_i^+]$ and $[H_e^+]$ are included. $\Delta\tilde{\mu}_{H^+}$ and $\Delta\Psi$ are calculated at each step from the ΔpH value using the constant *u*. The initial pH_e value is 6.9 [7]. The proton concentration in the matrix changes much more slowly than could be expected from the number of protons ejected from the matrix volume because of its high buffering capacity c_{buff}. It has been measured that c_{buff} equals 0.022 M H^+ per pH unit (assuming 1 μl matrix volume per mg of protein) [30]. The buffering is caused by a proton 'trapping' by proteins and lipids. The 'natural' capacity is equal to:

$$c_0 = (10^{-\text{pH}} - 10^{-\text{pH}-\text{dpH}})/\text{dpH} \qquad (14)$$

where dpH is a small change in pH. The buffering coefficient r_{buff} determines the efficiency of buffering and can be defined as follows:

$$r_{buff} = c_{buff}/c_0 \qquad (15)$$

It determines the intramitochondrial space buffering capacity. It is assumed that the cytosol space buffering capacity is R_{cm}-times higher. In the presented model for description of the ATP/ADP carrier kinetics values of Ψ_i and Ψ_e are needed – any, even fictitious, but a constant ratio of $-\Psi_i/\Psi_e$ is necessary. Taking into account the higher external capacity for cations (so the smaller displacing of the external electric potential from zero) we assume that $-\Psi_i/\Psi_e = R_{cm}$, $\Psi_i = \Delta\Psi \cdot R_{cm}/(1 + R_{cm})$, and $\Psi_e = \Psi_i - \Delta\Psi$. Of course, this is only the rough approximation. In fact, the Ψ_e value is relatively close to zero and can be neglected [27]. Additionally, it has been checked that our simulations are insensitive to this parameter.

The nonlinear dependence of the proton leak flux on $\Delta\Psi$ has been reported while the linear dependence on ΔpH has been obtained in some experiments [31,32]. From a number of different experimental results we applied the dependence obtained by O'Shea et al. [31] because of the sharp increase in proton conductance at a certain value of $\Delta\Psi$. This phenomenon can explain the great difference in the proton leak rate between states 3 and 4, when $\Delta\tilde{\mu}_{H^+}$ alters by a value less than 30 mV. The authors originally proposed an exponential dependence between the leak flux and $\Delta\Psi$. We find a better fit to the presented results for the sum of the exponential and the linear relationship, the latter being the same as for ΔpH. We obtain the following equation for the proton leak rate:

$$v_{LEAK} = k_{L1}(e^{k_{L2}\cdot\Delta\Psi} - 1) + k_{L3}\cdot\Delta\tilde{\mu}_{H^+} \qquad (16)$$

where, for the assumed cytochrome *c* concentration:

$k_{L1} = 2.1\cdot10^{-6}$ μM H^+ s^{-1}

$k_{L2} = 9.0\cdot10^{-2}$ mV^{-1}

$k_{L3} = 2.0\cdot10^{-2}$ μM H^+ mV^{-1} s^{-1}

k_{L2} is calculated from Ref. 31, and k_{L1} and k_{L3} are adjusted to obtain a proton flux intensity equal to about 25% of the proton pumping rate [17,18].

ATP synthetase

The ATP synthetase utilizes the protonmotive force for the synthesis of ATP from ADP and P_i. Magnesium complexes of adenine nucleotides (ATP_{mi}, ADP_{mi}) and monovalent phosphate (P_{iii}) are involved in this reaction. The ATP synthesis is coupled with the proton back-flow to the matrix. Different H^+/ATP stoichiometrics (n_A) have been reported (mostly from 2 to 3). We adjusted such an n_A value as would yield a very small displacement of the reaction from equilibrium (thermodynamic calculation is performed using the standard Gibbs (free energy change for ATP synthesis of -31.9 kJ M^{-1} [33]). For the value $n_A = 2.5$ a displacement from equilibrium of 2.64 is obtained, which

fulfils the required restrictions. A very similar $n_A + 1$ value for external ATP has been reported [34]. Of course, it would look better for heuristic reasons if n_A had an integer value. Nevertheless, a new inhibitor, almitrine, has been described recently [35] which can change this value. So, there is no reason for the ATP synthetase to have just an integer value of H^+/ATP stoichiometrics under physiological conditions. The kinetics of ATP synthetase is not entirely known, but probably the rate-limiting step is a product dissociation from the enzyme (a simple first-order reaction) [36]. It is proposed that two forms of the enzyme (bound with ATP and ADP) are at equilibrium. If the total enzyme concentration is denoted by E, ATP-bound one by E1, and ADP-bound one by E2 then $E = E1 + E2$. If we make two assumptions: (1) that the ratio of concentrations of these two forms of enzyme equals to the displacement from equilibrium γ ($E1/E2 = \gamma$), (2) that the dissociation rate constants k'_s for the two forms are the same (and thus $v = k'_s$ (E1–E2)), the following expression for the ATP synthesis rate v_{SYNT} can be easily obtained:

$$v_{SYNT} = k_s(\gamma - 1)/(\gamma + 1) \tag{17}$$

where $k_s = k'_s E$. The rate constant k_s is calculated using the initial rate of ATP synthesis $v_{SYNT} = (18v_{RESP} - v_{LEAK})/(n_A + (2R_{cm} - 1)/2R_{cm})$ and $\gamma = 10^{(n_A+1)\Delta\tilde{\mu}_{H+}/Z - \Delta G_P/S}$ values.

Adenine nucleotide, phosphate and magnesium systems

Some ligands in matrix and in cytosol bind magnesium ions Mg^{2+} (for example ATP, ADP, P_i, citrate). It is of some importance to know the concentrations of magnesium complexes with ATP and ADP because bound forms of adenine nucleotides participate in reactions catalyzed by ATP synthetase while free forms are translocated by an ATP/ADP carrier. Also in the adenylate kinase-catalyzed reaction complexed and free nucleotides take part. The concentration of magnesium and its main ligands in both extra- and intramitochondrial spaces were measured [37]. The free magnesium concentration $Mg_f = [Mg^{2+}]$ is essentially the same in the two compartments and amounts to about 380 μM. Total concentrations of main magnesium ligands and dissociation constants (K_D) for magnesium complexes are presented in Table I. The difference between dissociation constant values in the matrix and cytosol caused by the initial difference in pH is taken into account, although the pH-dependent changes in time are neglected for simplicity. Concentrations of free and complexed forms are calculated from the expressions:

$$X^n_{fy} = X^n_{ty}/(1 + Mg_{fy}/K_{Dny}) \tag{18}$$

$$X^n_{my} = X^n_{ty} - X^n_{fy} \tag{19}$$

TABLE I

Concentrations and dissociation constants of most important magnesium ligands [37]

Ligand	Cytosolic space		Mitochondrial space	
	concentration (μM)	K_D (μM)	concentration (μM)	K_D (μM)
ATP	2760	24	10400	17
ADP	315	347	5860	282
AMP	130	– [a]	–	–
P_i	3340	1180	16800	1176
Citrate	1200	270	5200	238
R (magnesium binding pool)	5550	710	34700	221

[a] K_D very high, practically all AMP in the free form.

where 'X^n' is the n-th ligand concentration ([X^n]) and the index 'y' denotes 'i' or 'e' indexes. The total magnesium concentration is calculated as follows:

$$Mg_{ty} = \sum_n X^n_{my} + Mg_{fy} \tag{20}$$

During the simulation the free magnesium concentration is recalculated at each step, using ten iterations in each step of the simulation:

$$Mg_{fy} = Mg_{ty}/\left(1 + \sum_n (X^n_{ty}/(Mg_{fy} + K_{Dny}))\right) \tag{21}$$

It has been reported that some of the cytosolic ADP is bound to the ADP-binding pool [38]. About 60% of ADP is not bound ('free ADP_e coefficient' $f_{ADP} = 0.6$). Thus, the free total concentration [ADP'_{te}] at the initial point is equal to $[ADP_{te}] \cdot f_{ADP}$. The dissociation constant K_{DB} is determined to be equal to 280 μM [38]. The free, bound and total ADP-binding pool concentrations are calculated respectively:

$$B_f = K_{DB}(1/f_{ADP} - 1) \tag{22}$$

$$B_{ADP} = ADP_{te}(1 - f_{ADP}) \tag{23}$$

$$B_t = B_{ADP} + B_f \tag{24}$$

At each step of simulation B_f is calculated in ten iterations:

$$B_f = B_t/(1 + ADP_{te}/(B_f + K_{DB})) \tag{25}$$

A linear approximation is not used because of the relatively small ADP-binding pool.

Inorganic phosphate can occur in the cell in two forms: monovalent and divalent. Only the former is co-transported with a proton by the phosphate carrier and its concentration is needed. The following relation

between monovalent $P_{i_{ay}}$ and total $P_{i_{ty}}$ concentration of inorganic phosphate was used [6]:

$$P_{i_{ay}} = P_{i_{ty}} / (1 + q_y) \tag{26}$$

where $q_y = 10^{(pH_y - pK_a)}$ and $pK_a = 6.8$.

Internal ATP utilization

It is assumed that ATP utilization has the activity per volume unit in the mitochondrial space equal to half that in the cytosolic space. Thus, the initial internal ATP consumption rate is equal to $v_{CONS} = (1/(2R_{cm})) \cdot v_{SYNT}$ and seems to be insignificant. This process is described by a single irreversible reaction with the Michaelis-Menten constant K_{MC} for ATP equal to 500 μM. This value is similar to the K_M constant of hexokinase (440 μM [39]). The V_{maxC} value is calculated from initial v_{CONS} and K_{MC} values. The adequate rate expression is:

$$v_{CONS} = V_{maxC} / (1 + K_{MC} / ATP_{ti}) \tag{27}$$

ATP/ADP carrier

Adenine nucleotides can be exchanged across the inner mitochondrial membrane by the ATP/ADP translocator. Two mechanisms of the ATP/ADP carrier function are proposed. According to the first one the enzyme catalyzes the exchange of adenine nucleotides across the inner mitochondrial membrane in a single-step reaction with the creation of the ternary complex [40,41]. The kinetic model based on this mechanism was applied by Holzhütter et al. [6]. Recent studies suggest, however, rather different kinetics (Klingenberg [42]). The translocation occurs there by subsequent binding of the adenine nucleotide from one side of the membrane, the conformation change of the enzyme linked with the nucleotide exposition from the other side, releasing the nucleotide at this side and coming back with another molecule. It has been reported that the exchange rate depends on $\Delta\Psi$ and that the enzyme is saturated with adenine nucleotides (K_M less than 5 μM [42]). ATP has its relative affinity a_r to the binding site of the carrier comparing with ADP equal to 0.6. Because of the enzyme binding site charge the ADP molecule is translocated as a neutral one, while ATP has one negative charge. In the exchange reaction only magnesium-free nucleotides take part.

We have developed a kinetic model which attempts to describe this mechanism. The concentration of the matrix-exposed form of enzyme is denoted by C_i and the cytosol-exposed one by C_e. The sum $C = C_i + C_e$ is established as equal to 1. Reactions of the adenine nucleotides translocation from the two compartments are described as follows:

$$v_i = k_i \cdot C_i \tag{28}$$

$$v_e = k_e \cdot C_e \tag{29}$$

Some assumptions are made: (1) The translocation rate is equal for both adenine nucleotides in both directions, if electrical potential is absent (equal rate coefficients s_i and s_e). (2) In the presence of $\Delta\Psi$ the rate of the ATP_y translocation depends linearly on $10^{\Psi_y/Z}$ (as on the chemical potential). (3) Because of saturation the ratio of ATP to ADP molecule quantities bound from the given side of the membrane to the enzyme depends only on the relative concentrations and affinities of these nucleotides. Taking into consideration the above assumptions we obtain:

$$k_y = s_y \cdot \left(a_r ATP_{fy} 10^{\Psi_y/Z} + ADP_{fy}\right) / \left(a_r ATP_{fy} + ADP_{fy}\right) \tag{30}$$

$$C_e / C_i = e_{ei} = k_i / k_e \tag{31}$$

$$s_i = s_e \text{ (rate coefficients)} \tag{32}$$

$$C_i = C / (e_{ei} + 1) \tag{33}$$

and finally the exchange rate is:

$$v_{EXCH} = k_{exch} C_i \left(a_r ATP_{fi} 10^{\Psi_i/Z} / (a_r ATP_{fi} + ADP_{fi})\right) - C_e \left(a_r ATP_{fe} 10^{\Psi_e/Z} / (a_r ATP_{fe} + ADP_{fe})\right) \tag{34}$$

because ATP/ATP and ADP/ADP exchange can be omitted. The k_{exch} constant is calculated from the initial ATP/ADP exchange rate v_{EXCH} which is equal to the initial ATP synthesis rate v_{SYNT} multiplied by a factor $(R_{cm} - 1)/R_{cm}$. The translocation rate is then controlled by two factors: (1) the electrical potential, (2) the relative ATP and ADP concentration from the two sides of the membrane. At the initial point of the simulation the carrier is displaced from equilibrium approx. 28-times, which corresponds very well to the value of 30 reported in Ref. 42.

Phosphate carrier

The phosphate carrier catalyzes the co-translocation of monovalent inorganic phosphate with a proton across the inner mitochondrial membrane. It is accepted that the phosphate carrier is near equilibrium, thus, the displacement from equilibrium equal to 3.7 calculated on the thermodynamic basis in the model at the initial point seems to be acceptable. Using this value and the initial rate of the phosphate carrier-catalyzed reaction $v_{PIIN} = v_{EXCH}$, the final expression for translocation rate of inorganic phosphate is:

$$v_{PIIN} = k_p \cdot H_e \cdot P_{i_{ae}} - k_{bp} \cdot H_i \cdot P_{i_{ai}} \tag{35}$$

Adenylate kinase

This enzyme present in the cytosolic space (strictly between the inner and outer mitochondrial membrane), catalyzes the very close to equilibrium reaction of transforming two ADP molecules into one ATP and one AMP molecule [43]. One of the two ADP molecules and the ATP molecule are complexed with magnesium, while other reagents are in magnesium-free forms, so the reaction appears as follows:

$$ADP_{me} + ADP_{fe} \leftrightarrow ATP_{me} + AMP_{fe}$$

The equilibrium constant is calculated from initial concentrations of reagents:

$$K_{ak} = ADP_{me}ADP_{fe}/(ATP_{me}AMP_{fe}) \tag{36}$$

The apparent equilibrium constant related to total concentrations of reagents is calculated using the simplified expression from Ref. 6:

$$K'_{ak} = ADP_{te}ADP_{te}/(ATP_{te}AMP_{te})$$

$$= K_{ak}(K_{DADPe} + Mg_{fe})^2/(K_{DADPe}(K_{DATPe} + Mg_{fe})) \tag{37}$$

Two pool variables are used as in Ref. 6:

$$A_{TDM} = ATP_{te} + ADP_{te} + AMP_{te} \tag{38}$$

$$A_{2TD} = 2ATP_{te} + ADP_{te} \tag{39}$$

and, because of binding of part of the ADP in cytosol:

$$A'_{TDM} = A_{TDM} - B_{ADP} \tag{40}$$

$$A'_{2TD} = A_{2TD} - B_{ADP} \tag{41}$$

Now, total external adenine nucleotide concentrations at each iteration can be obtained:

$$a = 4 - K'_{ka}$$

$$b = K'_{ka}(A'_{TDM} - A'_{2TD}) + 4A'_{2TD}$$

$$c = (A'_{2TD})^2$$

$$ATP_{te} = (b/2a)\left(1 - \sqrt{1 - 4ac/b^2}\right) \tag{42}$$

$$ADP'_{te} = A'_{2TD} - 2ATP_{te} \tag{43}$$

$$AMP_{te} = A'_{TDM} - ATP_{te} - ADP'_{te} \tag{44}$$

External ATP utilization

A description of this process is very similar to the internal ATP consumption one, the value of K_{MU} amounting to 500 μM also. V_{maxU} is obtained from the initial external ATP utilization rate $v_{UTIL} = v_{EXCH}$. The rate expression is:

$$v_{UTIL} = V_{maxU}/(1 + K_{MU}/ATP_{te}) \tag{45}$$

TABLE II

The set of differential equations

Equation number	Equation
I	$\dot{O}2 = v_{b2} - v_2 = -v_{RESP}$
II	$\dot{A}1 = v_2 - v_{b2} - v_4$
III	$\dot{A}2 = v_4 + v_{b1} - v_1$
IV	$\dot{A}3 = v_1 + v_{b2} - v_{b1} - v_2$
V	$\dot{N}h = v_{DEHY} - 0.5 \cdot v_{OXID}$
VI	$\dot{H}_i = -(18 \cdot v_{RESP} - n_A v_{SYNT} - u \cdot v_{EXCH} - (1-u) \cdot v_{PHN} - v_{LEAK}) \cdot R_{cm} \cdot R_{sc}/r_{buff}$
VII	$\dot{H}_e = -\dot{H}_i/R_{cm}$
VIII	$\dot{ATP}_{ti} = (v_{SYNT} - v_{EXCH} - v_{CONS}) \cdot R_{cm} \cdot R_{sc}$
IX	$\dot{ADP}_{ti} = -\dot{ATP}_{ti}$
X	$\dot{P}_{i_{ti}} = (v_{PHN} + v_{CONS} - v_{SYNT}) \cdot R_{cm} \cdot R_{sc}$
XI	$\dot{A}_{2TD} = (v_{EXCH} - v_{UTIL}) \cdot R_{sc}$
XII	$\dot{P}_{i_{te}} = (v_{UTIL} - v_{PHN}) \cdot R_{sc}$

The above kinetics corresponds to the conditions without glycolysis (no additional ATP supply) and gluconeogenesis (ATP utilization essentially independent on the ATP/ADP ratio). We will deal with these metabolic variants in a subsequent paper. In this work, we describe conditions corresponding to the resting cell suspension with the fatty acids β-oxidation being (immediately or through the tricarboxylate acids cycle) the main source of reducing equivalents.

Set of differential equations

The set of differential equations used in this simulation is presented in Table II. It contains 12 differential equations (10 independent ones). They describe changes in time of a number of parameter values, while the values of other parameters are calculated at each iteration step from the latter.

Flux control coefficients

The metabolic control theory successfully describes the sharing of control over a metabolic process (including the oxidative phosphorylation) between the enzymes (reactions) taking part in it [2,44]. The parameter which determines the degree of control of a given enzyme (or process, for example, proton leak) over the whole considered metabolic pathway is the flux control coefficient. It is defined as follows [44]:

$$C_{E_i}^{J_m} = (\delta J_m/J_m)/(\delta E_i/E_i) \tag{46}$$

In other words, the flux control coefficient describes what will be a relative change in the value of the flux J over the metabolic pathway m under the influence of a small relative change in the concentration (activity) of the enzyme, which catalyzes the reaction i. It has been

demonstrated that the sum of flux control coefficients for all enzymes of the given pathway is equal to 1 (the so-called summation property). We perform the small changes in enzyme activity in the model by diminishing their rate constants by a relative factor of 10^{-4}. Then the relative change in the respiratory rate (oxygen consumption flux) is calculated after achieving the steady state by the system. Of course, simulations of flux control coefficients are performed for the constant, initial, oxygen concentration. Thus, it is possible to obtain the flux control coefficient for the most important enzymes of oxidative phosphorylation.

Results and Discussion

Changes in time of the values of six groups of chosen parameters are drawn in six diagrams in Fig. 2. The time period of the simulation is 600 s, including 400 s of oxygen consumption and anaerobiosis and 200 s after oxygen pulse (240 μM).

In Fig. 2a the oxygen concentration against time is drawn. The value of this parameter falls monotonously from 240 μM to zero, with a little band before anaerobiosis. The calculated apparent Michaelis-Menten constant for oxygen amounts to $K_m = 0.55$ μM. This value is close to the experimental one, which is about 0.5 μM [11].

Fig. 2b presents time-courses of concentrations of three forms of cytochrome oxidase (see Ref. 1). The A3 form, which can bind oxygen has a very low relative concentration at high oxygen concentrations. Its value increases slowly when oxygen pressure diminishes in order to maintain a respiratory rate as constant as possible. The A3 concentration 'explodes' very sharply at the beginning of anaerobiosis, when the control over respiration 'breaks down'. The A2 form, which serves as 'substrate' of the A3 form, increases its concentration in time to maintain the A3 supplying rate at an adequate level. After achieving anaerobiosis the A2 concentration ceases to increase and starts to fall sharply. This moment is a good indicator of the 'breaking down' of the control. Because of the 'moiety conservation' property, the A1 form concentration decreases in time in the whole range of oxygen concentration. In this case the flux over the whole cytochrome oxidase cycle can be kept almost constant, since A1 is able to be transformed into A2 in one of two parallel ways (see Refs. 8–10). If the internal proton concentration increases with a diminution of oxygen concentration (when the proton-motive force decreases) the

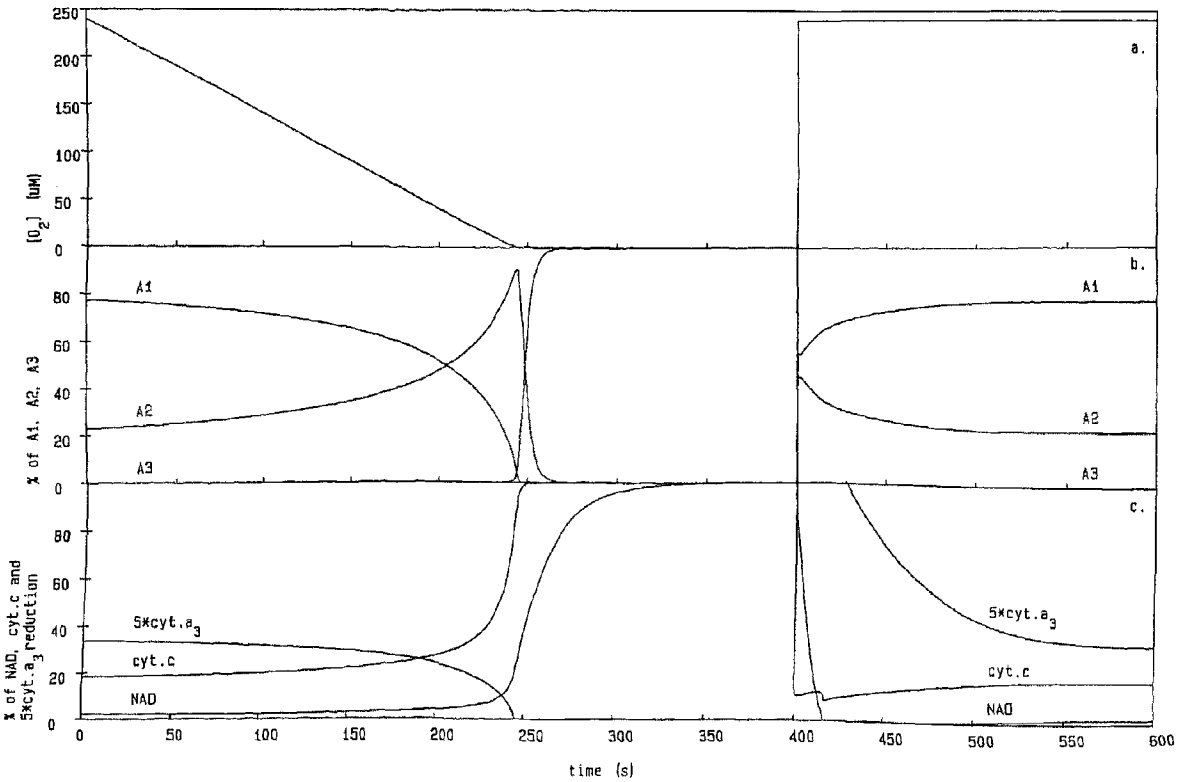

Fig. 2. Time-courses of chosen system parameters. After 400 s the oxygen pulse is added.

greater relative flux flows through the faster mechanisms because of a change in the K_3 constant value (and the middle point potential of cytochrome a_3 [9,21]). It leads to an increase in the value of the phenomological k_k constant. Thus, the cytochrome oxidase exhibits a very precise regulation of the respiratory rate value.

Fig. 2c shows changes in the reduction level of NAD, cytochrome c, and cytochrome a_3 in time. These changes (increase in the reduction of NAD and cytochrome c, decrease in the cytochrome a_3 one) are slight at high oxygen concentrations and become sharp in the region in which the oxygen concentration is equal to about K_m. The increase in the reduced form concentration of cytochrome c [cyt. c^{2+}] is due to driving of the cytochrome oxidase cycle during the consumption of oxygen (cyt. c^{2+} is the substrate of two reactions in this cycle [8,9]). The cytochrome c reduction level is affected by the thermodynamic span between NAD and cytochrome c (determined by the proton gradient across the inner mitochondrial membrane) and by the difference between substrate dehydrogenation and cytochrome c oxidation rates. The second factor causes NAD to follow cytochrome c in the increase in the reduction level. The level of cytochrome a_3 reduction reflects the absolute intensity of the faster of two alternative ways of A1 → A2 transition divided by cytochrome c concentration (its relative intensity increases in time). After the oxygen pulse the time-courses of NAD and cytochrome c reduction levels (similarly as cytochrome oxidase form concentrations) exhibit a very fast initial phase of return near the previous level (at high $[O_2]$) with a slight overshoot. The values of these parameters then slowly stabilize at the steady state level.

The diagram in Fig. 2d describes the time-course of $\Delta\tilde{\mu}_{H^+}$. It can be seen that the proton-motive force is essentially constant at high oxygen concentrations. After the onset of anaerobiosis it decreases very suddenly to about 140 mV and then diminishes at a moderate rate. The sharp phase is probably due to the rapid decrease in the rate of the proton pumping by the respiratory chain while the moderate rate phase reflects the proton leak, ATP utilization ($\Delta\tilde{\mu}_{H^+}$ is in equilibrium with the phosphorylation potential owing to the ATP synthetase function) and the ATP/ADP exchange together with the P_i/H^+ co-transport. The proton-motive force disappears almost entirely after a short time which is caused by the non-glycolytic conditions. After the oxygen burst the time-course of the

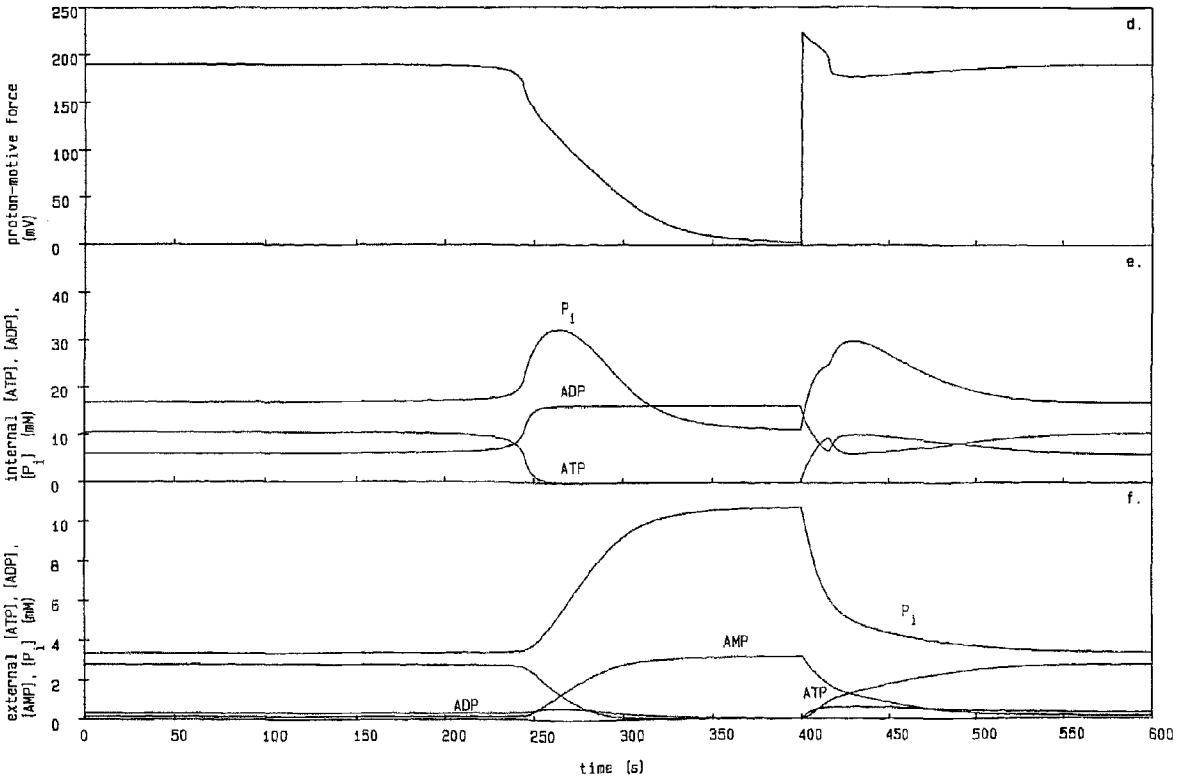

Fig. 2 (continued).

proton-motive force exhibits the overshoot characteristics which were earlier found experimentally [7]. The highest potential at a peak equal to about 230 mV is observed. It has been explained [6] by a lag-phase kinetics of ATP synthetase reported in the literature [45]. The simulation shows that this hypothesis is not a necessity for obtaining such a behaviour of the system. The obtained dependence can be explained by other internal system properties, probably mainly by the very fast action of the respiratory chain, which utilizes stored reduced redox equivalents and by the limited ATP synthetase capacity far from equilibrium. If an upper limit is imposed for the respiratory chain activity, which is equal to the doubled initial activity (a rather severe limitation), the results are similar, though the overshoot is smaller.

Fig. 2e illustrates the behaviour of the internal phosphorylation system. Concentrations of ATP_i, ADP_i and P_ii, essentially constant at high oxygen concentrations, change quickly after oxygen depletion. The curves of ATP concentration decrease and that of ADP increase are symmetrical with respect to the horizontal line (moiety conservation property). The phosphate concentration increases owing to the ATP hydrolysis to the point of zero oxygen concentration and then decreases in order to maintain the equilibrium with the diminishing $\Delta\tilde{\mu}_{H^+}$ (phosphate carrier near equilibrium). After reoxygenation, the concentrations of the mentioned compounds exhibit an overshoot and then slowly return to steady-state values. The 'double' overshoot of the inorganic phosphate concentration is caused subsequently by the proton-motive force overshoot and by a decay of that of adenine nucleotides.

In Fig. 2f time-courses of concentrations of ATP_e, ADP_e, AMP_e and P_{ie} are presented. Typically, changes long before anaerobiosis are very small. Oxygen depletion initially causes a relatively rapid increase in P_i, AMP and ADP concentrations, while that of ATP decreases. But in a short time [ADP] falls because of the moving of the adenylate kinase reaction towards synthesis of AMP and ATP. The latter is immediately hydrolyzed, this shifting the reaction in the same direction. The great increase in the external phosphate concentration is the result of ATP utilization and reestablishment of a new equilibrium between the phosphate gradient and proton gradient across the inner mitochondrial membrane. After reoxygenation the external phosphorylation potential slowly stabilizes at the steady-state value.

From the results of the performed simulation it can be seen that only cytochrome oxidase is distinctly sensitive to the oxygen concentration in its whole range. Other components of the system have almost constant concentrations at higher oxygen levels. The respiratory chain, which is in direct contact with cytochrome oxidase, donating electrons for it, exhibits intermediate behaviour. This is, understandable, in order to maintain the constant ATP utilization (not dependent on $[O_2]$).

A 'hot region' can be observed when the oxygen concentration attains zero. It is characterized by very rapid changes in all the mentioned parameter values (the reduction level of the respiratory chain and cytochrome oxidase, the size of the proton-motive force, intra- and extramitochondrial phosphorylation potential). This region, most clearly expressed for NAD, cytochrome *c* and cytochrome oxidase is due to the 'breakdown' of the control over oxidative phosphorylation. By 'breakdown' we mean the situation when the system capacity for compensation of the oxygen concentration decrease is exhausted. The system can no longer ensure a constant respiratory rate because of the moiety conservation property of components of the respiratory chain. Nevertheless, this property makes possible a very precise regulation in almost the whole range of oxygen concentration [28]. There are four main pools, which exhibit (strictly or approximately) the feature: the respiratory chain (NAD, UQ, and cytochrome *c* pools), the proton pool ($[H_i] + [H_e] \cdot R_{cm}$), the internal adenine nucleotide pool ($[ATP_i] + [ADP_i]$), and the external adenine nucleotide pool ($[ATP_e] + [ADP_e] + [AMP_e]$). These pools are connected by proton pumps (complexes I, III, IV), ATP synthetase and the ATP/ADP carrier. There are two inputs of the system: the substrate dehydrogenation, which affects the respiratory chain, and ATP utilization, which contacts the external adenine nucleotide pool.

A good semi-quantitative agreement can be found between simulated time-courses of cytochrome *c* reduction and oxygen concentration and experimentally obtained ones for the cell suspension [12] (for example about 20% of the cytochrome *c* reduction at high oxygen concentrations). An exact comparison is not possible since in the cited works some parameters were not measured. Unfortunately, changes in time of other parameters in the cell suspension are not available in the literature.

The steady state model (Wilson et al. [4–6]) described the cytochrome oxidase kinetics as a function of the external $[ATP]/[ADP][P_i]$ ratio. Such a dependence is used in the presented model. It can be regarded only as a 'black box' relationship, but it has been verified by the good agreement with experiments [9–13]. The proof that such a simplification is justified is constituted by the good agreement of the simulated K_m value with the one obtained experimentally.

Of great importance is not only how the system behaves in time, but also which of its components plays a major role in regulation of the intensity of the metabolic flux flowing through the system. The metabolic control theory is a good tool for this pur-

TABLE III

Flux control coefficients for main reactions of oxidative phosphorylation

All values measured experimentally are taken for the respiratory rate equal to 40–50% of its maximal value

Enzyme (reaction)	Physiological conditions simulation	Artificial conditions simulation	Experimental results (Ref. 36)
External ATP utilization	0.56	0.59	0.51
Substrate dehydrogenation	0.23	0.11	0.09
ATP/ADP carrier	0.04	0.01	0.18
Proton leak	0.20	0.19	0.32 (?)
Cytochrome oxidase	0.01	0.08	about 0.05–0.10 [a]
Internal ATP consumption	0.02	0.02	?
Phosphate carrier	−0.03	0.00	?
ATP synthetase	−0.03	0.00	?
Sum	1.00	1.00	> 1.10 (about 1.20 ?)

[a] Extrapolated from a value of 0.17 in state 3.

pose. Flux control coefficients for all reactions described by rate constants were calculated, the results being presented in Table III (first column). It can be seen that the control is not shared uniformly: three reactions 'keep' a majority of it. More than 20% of the entire control strength is at the substrate dehydrogenation. It is obvious that the respiration substrate delivery takes part in the regulation of the whole process. More than half of the control is linked with the external ATP utilization. If we take into account the internal ATP consumption as well, we see that about 58% of the control is performed by the cell energy demand. Such a statement seems to be logical, because ATP delivery for anabolic reactions and ion transport is the primary 'purpose' of the whole system described in the model presented. About 20% of the control is at the proton leak. It seems to be a direct result of the established relative intensity of the proton leak in relation to the proton pumping activity. Other components of the oxidative phosphorylation system have flux control coefficients near zero and virtually do not participate in the control.

These results are in partial contradiction with the experimental results reported by Groen et al. [46]. In Table III (third column) flux control coefficients obtained in the cited work for a respiratory rate equal to about 40–50% of its maximal value are presented. While the control strength of external ATP utilization is essentially similar, that for substrate dehydrogenation is much smaller, and that for the ATP/ADP carrier has a distinctly higher value. The relatively higher flux control coefficient was measured for proton leakage. Hence, the pattern of the control strength sharing appears to be quite different from that in the simulations presented. However, it must be emphasized that in Ref. 46 unphysiological conditions were established. An artificial substrate dehydrogenation system was used, consisting of succinate dehydrogenase and a dicarboxylate carrier. Succinate dehydrogenase catalyzes the reversible reaction and in the experiment was probably near thermodynamic equilibrium with its substrate (succinate) [22]. This is in contrast to the situation involving intact cells, where all substrate dehydrogenation is regulated by irreversible reactions [23] (for example all the flux through the citric acid cycle is mainly controlled by pyruvate, 2-oxoglutarate and isocitrate dehydrogenase). If another substrate is used (glutamate + malate), practically no control of the ATP/ADP carrier can be observed [47,48] (the authors originally proposed that the reason for the difference was the method of mitochondria isolation). Thus, in the previously cited experiment, a part of the control can be shifted from substrate dehydrogenation to other reactions. Further, a relatively high concentration of the external P_i (10 mM) and a rather low one of the external adenine nucleotide pool (1 mM) were used (in relation to cell conditions, see Table I). In order to maintain the external phosphorylation potential, the $[ATP_e]/[ADP_e]$ ratio must be relatively higher. This decreases the $[ADP_e]$ participation in the external adenine nucleotide pool and inhibits the ATP_i/ADP_e exchange catalyzed by the adenine nucleotide carrier. The lower external ATP concentration is relatively nearer the K_m constant for hexokinase, which slightly decreases the control strength of ATP utilization. The high inorganic phosphate concentration decreases the exchange rate in relation to the respiratory rate (the former is sensitive to [ATP]/[ADP] ratio, the latter to the $[ATP]/[ADP][P_i]$ ratio [49]), which moves the next amount of control to ATP/ADP translocase. The reversible substrate dehydrogenation, partially inhibited adenine nucleotide carrier, and action of only two coupling sites decrease the relative value of the oxidative phosphorylation and increase $\Delta\bar{\mu}_{H^+}$, which enhances control by the proton leak. Moreover, the summation property is not fulfilled. The sum of the flux control coefficients in the experiment is higher than 1.1 (since control strength for some reactions was not measured, the sum can amount to even 1.2). It is possible that it is due to overestimation of the flux control coefficients for the proton leak and ATP/ADP carrier. In the second column of Table III flux control coefficients that were obtained by a simple modification of the dynamic model to the artificial conditions

are shown. Two coupling sites are applied here and the external adenine nucleotide pool from the experiment is used. The extramitochondrial parameters are described in the suspension volume instead of the cell volume. A better agreement can now be found between the mentioned experiment and 'mitochondrial conditions' simulation: the flux control coefficients for ATP utilization, substrate dehydrogenation, and, roughly speaking, the proton leak are similar. Moreover, in spite of the lack of a measured value of the control strength for cytochrome oxidase in state $3_{(1/2)}$, its value of 0.17 in state 3 can be discussed. Because the flux control coefficient for cytochrome oxidase probably increases with the state 4 → state 3 transition the simulated value of 0.08 in state $3_{(1/2)}$ agrees well with the one measured in state 3. An important different still exists for the adenine nucleotide carrier. Gellerich et al. [50] obtained essentially no control for the adenine nucleotide carrier in the hexokinase system at the median-rate respiration. They suggested that the high value measured by Groen et al. was due to the high (25%) relative change in enzyme activity by carboxyactractyloside titration. We suppose that the second reason is the relatively slow (some minutes) return of the system to equilibrium after a disturbance, as we obtain in our model. Thus, during the period of measurement, the system might not achieve equilibrium. Probably this is due to the large extramitochondrial adenine nucleotides used and to the fact that the system returns to equilibrium slower when it is nearer the equilibrium. This return rate is essentially condition-dependent (external phosphorylation potential, magnesium ions concentration); it can partially explain differences between the two experiments mentioned. The high flux control coefficient for ATP/ADP exchange (0.26) was obtained in hepatocytes with lactate + pyruvate as substrate [51]. However, under those conditions, gluconeogenesis is the main ATP-consuming process. Its intensity is strongly [ATP]/[ADP]-dependent (see the discussion in Ref. 50). The simulation performed for such conditions gives results which are similar to those in the cited work (unpublished data). In this case, it may be concluded that the adenine nucleotide carrier does not keep the essential part of the control under the conditions simulated in this work.

A very useful tool for studying the control of the oxidative phosphorylation is the 'top-down' approach to the metabolic control theory [52]. It deals with flux control coefficients of whole branches or 'subpathways', not of particular enzymes. In two excellent works [18,53] these coefficients were measured for the oxidation system (substrate dehydrogenation, respiratory chain, cytochrome oxidase), the phosphorylation system (ATP synthetase, ATP/ADP carrier, phosphate carrier, ATP utilization), and the proton leak in both mitochondria and cell conditions. The results are compared with our simulations in Table IV. Surprisingly good agreement can be observed, proving, in our opinion, that at least general features of the model are correct.

TABLE IV

Flux control coefficients over the oxygen consumption flux of the oxidation system, phosphorylation system and proton leak – the 'top-down' approach to the metabolic control theory

The experimental values for mitochondria are taken for the respiratory rate equal to about 50% of its maximal value and those for cells for starved ones

Pathway	Mitochondria conditions		Cell conditions	
	simulation	experiment [53]	simulation	experiment [18]
Oxidation	0.19	0.15	0.24	0.27
Phosphorylation	0.62	0.65	0.56	0.57
Proton leak	0.19	0.20	0.20	0.16

In light of the above discussion we propose that the main part of the control over the oxidative phosphorylation in simulated conditions (intact cells, state $3_{(1/2)}$, lack of glycolysis and gluconeogenesis) is shared between inputs of the system: the ATP utilization and substrate dehydrogenation (with domination of the former), and the proton leak. Such a control pattern ensures the good response for the cell energy demand.

The model presented is based on some advantageous properties of previous models. From Ref. 1 was taken the verified quantitative description of cytochrome oxidase function and the rather kinetic than thermodynamic paradigm of model building. In Ref. 6 the description of magnesium complexes and the adenylate kinase, and, of course, application of the proton-motive force instead of the 'black box' relationship was accepted. The current model has some new features: new descriptions of the ATP synthetase, and the ATP/ADP carrier function, the non-linear dependence of the proton leak flux on $\Delta\Psi$, the calculation of flux control coefficients, the internal and external ATP utilization and intact cell conditions. There are two main disadvantages of the model. Many rate constants are not obtained experimentally but calculated on the assumption of the validity of the model. It has a limited possibility of exact quantitative comparison with experimental results reported up till now.

For presentation of the model, our purpose was to attempt to gain a more profound understanding of what 'keeps' the control over the process of oxidative phosphorylation under physiological conditions and in what way. We hope that at least partially this task has been carried out. Of course, in the future, the model will have to be adjusted to new knowledge and to be verified experimentally.

References

1 Korzeniewski, B. and Froncisz, W. (1989) Studia Biophysica 132, 173–187.
2 Brand, M.D. and Murphy, M.P. (1987) Biol. Rev. 62, 141–193.
3 Westerhoff, H.V. and Van Dam, K. (1987) Thermodynamics and Control of Biological Free-Energy Transduction, Elsevier, Amsterdam.
4 Bohnensack, R. (1981) Biochim. Biophys. Acta 634, 203–218.
5 Bohnensack, R., Küster, U. and Letko, G. (1982) Biochim. Biophys. Acta 680, 271–280.
6 Holzhütter, H.-G., Henke, W., Dubiel, W. and Gerber, G. (1985) Biochim. Biophys. Acta 810, 252–268.
7 Ogawa, S. and Lee, T.M. (1984) J. Biol. Chem. 259, 10004–10011.
8 Wilson, D.F., Owen, C.S. and Holian, A. (1977) Arch. Biochem. Biophys. 182, 749–762.
9 Wilson, D.F., Owen, C.S. and Erecińska, M. (1979) Arch. Biochem. Biophys. 195 (2), 494–504.
10 Wilson, D.F. and Nelson, D. (1985) in Mathematics and Computers in Biomedical Application (Eisenfeld, J. and DeLisi, C., eds.), pp. 119–124, Elsevier/North-Holland, Amsterdam.
11 Wilson, D.F. and Erecińska, M. (1985) Chest 88, 229s.
12 Wilson, D.F., Erecińska, M., Drown, C. and Silver, J.A. (1979) Arch. Biochem. Biophys. 195, 485–493.
13 Wilson, D.F., Rumsey, W.L., Green, T.J. and Vanderkooi, J.M. (1988) J. Biol. Chem. 263 (6), 2712–2718.
14 Brand, M.D. (1990) Biochim. Biophys. Acta 1018, 128–133.
15 Wojtczak, L., Bogucka, K., Duszyński, J., Zablocka, B. and Zólkiewska, A. (1990) Biochim. Biophys. Acta 1018, 177–181.
16 Gear, C.W. (1971) Numerical Initial Value Problems in Ordinary Differential Equations, Prentice-Hall, Englewood Cliffs.
17 Nobes, C.D., Brown, G.C., Olive, P.N. and Brand, M.D. (1990) J. Biol. Chem. 265 (22), 12903–12909.
18 Brown, G.C., Lakin-Thomas, P.C. and Brand, M.D. (1990) Eur. J. Biochem. 192, 355–362.
19 Akerboom, T.P.M., Bookelman, H. and Zuurendonk, P.F. (1978) Eur. J. Biochem. 84, 413–420.
20 Ernster, L. (1984) Bioenergetics (in New Comprehensive Biochemistry, Vol. 9), Elsevier/North-Holland, Amsterdam.
21 Papa, S. (1988) in Oxidases and Related Redox Systems (King, T.E., Mason, H.S. and Morrison, M., eds.), Alan R. Liss, New York.
22 Gerville, G.D. (1966) in Regulation of Metabolic Processes in Mitochondria (Tager, J.M., Papa, S., Quagliariello, E. and Slater E.C., eds.), Elsevier, Amsterdam.
23 Hassinen, J.E. (1986) Biochim. Biophys. Acta 853, 135–151.
24 Plant, G.W.E. and Aogaichi, T. (1968) J. Biol. Chem. 243 (21), 5572–5583.
25 McCormack, J.G. and Denton, R.M. (1979) Biochem. J. 180, 533–544.
26 Erecińska, M., Veech, R.L. and Wilson, D.F. (1974) Arch. Biochem. Biophys. 160, 412–421.
27 Nicholls, D.G. (1982) Bioenergetics, Academic Press, London.
28 Reich, J.G. and Selkov, E.E. (1982) Energy Metabolism of The Cell, A Theoretical Treatice, Academic Press, London.
29 Duszyński, J., Bogucka, K. and Wojtczak, L. (1984) Biochim. Biophys. Acta 767, 540–547.
30 Mitchell, P. and Moyle, J. (1967) Biochem. J. 104, 588–600.
31 O'Shea, P., Petrone, G., Casey, R.P. and Azzi, A. (1984) Biochem. J. 219, 719–726.
32 Krishnamoorthy, G. and Hinkle, P.C. (1984) Biochemistry 23, 1640–1645.
33 Guynn, R.W. and Veech, R.L. (1973) J. Biol. Chem. 248, 6966–6972.
34 Kauppinen, R. (1983) Biochim. Biophys. Acta 725, 131–137.
35 Rigoulet, M., Fraisse, L., Ouhabi, R., Guerin, B., Frontaine, R. and Levevre, X. (1990) Biochim. Biophys. Acta 1018, 91–97.
36 Hatefi, Y., Ragan, C.J. and Galante, Y.M. (1985) in The Enzymes of Biological Membranes, Vol. 4 (Martinosi, A.N., ed.), Plenum Press, New York.
37 Corkey, B.E., Duszyński, J., Rich, T.J., Matschinsky, B. and Williamson, J.R. (1986) J. Biol. Chem. 261, 2567–2574.
38 Gankema, A.K., Groen, A.K., Wanders, R.J.A. and Tager J.M. (1983) Eur. J. Biochem. 131, 447–451.
39 Easterby, J.S. and O'Brien, M.J. (1973) Eur. J. Biochem. 38, 201–211.
40 Cleland, W.W. (1963) Biochim. Biophys. Acta 67, 104–137.
41 Duyckaerts, C., Sluse-Goffart, C.M., Fux, J.-P., Sluse, F.E. and Liebeq, C. (1980) Eur. J. Biochem. 106, 1–6.
42 Klingenberg, M. (1985) in The Enzymes of Biological Membranes, Vol. 4 (Martinosi, A.N., ed.), Plenum Press, New York.
43 Blair, J.M.D. (1970) Eur. J. Biochem. 13, 384–390.
44 Kacser, H. and Porteous, J.W. (1987) Trends Biochim. Sci. 12, 5–14.
45 Vasilyeva, E.A., Fitin, A.F., Minkov, J.B. and Vinogradov, A.D. (1980) Biochem. J. 188, 807–815.
46 Groen, A.K., Wanders, R.J.A., Westerhoff, H.V., Van der Meer, R. and Tager, J.M. (1982) J. Biol. Chem. 257 (6), 2754–2757.
47 Forman, N.G. and Wilson, D.F. (1983) J. Biol. Chem. 258 (14), 8649–8655.
48 Holian, A., Owen, C.S. and Wilson, D.F. (1977) Arch. Biochem. Biophys. 181, 164–171.
49 Wilson, D.F. (1982) in Membranes and Transport (Martinosi, A.N., ed.), pp. 349–355, Plenum Press, New York.
50 Gellerich, F.N., Bohnensack, R. and Kunz, W. (1983) Biochim. Biophys. Acta 722, 381–391.
51 Tager, J.M., Groen, A.K., Wanders, R.J., Duszyński, J., Westerhoff, H.V. and Vervoorn, R.C. (1983) in Isolation Characterization and Use of Hepatocytes (Harris, R.A. and Cornell, N.W., eds.), pp. 313–322, Elsevier, Amsterdam.
52 Brown, G.C., Hafner, R.P. and Brand, M.D. (1990) Eur. J. Biochem. 188, 321–325.
53 Hafner, R.P., Brown, G.C. and Brand, M.D. (1990) Eur. J. Biochem. 188, 313–319.